International Journal of Automotive Technology, Vol. 23, No. 2, pp. 389–401 (2022)
DOI 10.1007/s12239–022–0036–8

pISSN 1229–9138/ eISSN 1976–3832

CRASHWORTHINESS OPTIMIZATION OF IMPACT ATTENUATORS CONSTRUCTED OF POLYURETHANE FOAM

Amr Shaaban* and Adel Moneb Elsabbagh

Design and Production Engineering Department, Faculty of Engineering, Ain Shams University, Cairo 11517, Egypt

(Received 30 March 2021; Revised 14 June 2021; Accepted 10 August 2021)

ABSTRACT–This paper examines the crashworthiness optimization of an impact attenuator constructed of polyurethane (PUR) foam used in racing vehicles. Different design variables are investigated such as the mechanical properties associated with each PUR density and the attenuator topology. Analytical method is employed to model the behavior of the PUR, while finite element (FE)-simulation using LS-Dyna4.3© is conducted to evaluate the performance of the attenuator. The evaluation criteria in this study are the average and maximum acceleration throughout the impact period. The FE-results reveal that the PUR of 80 kg/m^3 is the most suitable, and experimental test is conducted for verification. The design of the attenuator is then modified by adding an internal cavity to provide a homogeneous cross-sectional area along the attenuator length. Size optimization analysis is carried out to attain stable acceleration values with the least average. Two approaches are considered for the design of the internal cavity, namely constant thickness and varied thickness. Various designs, each of specific cavity size and PUR density, are tested and the results are presented against each other. The varied thickness design with 30 mm base thickness and 145 kg/m^3 has proved to be the optimum design.

KEY WORDS : Crashworthiness design, Crashworthiness optimization, Polyurethane foam, Energy absorbing structures, Impact attenuator, Mean crash force

1. INTRODUCTION

Polyurethane (PUR) foams have had numerous applications for the past few decades because of their unique properties (Doyle, 1971; Ferrigno, 1967; Oertel and Abele, 1994; Szycher, 2012). There is a wide range of PUR foam densities which can be controlled during the manufacturing process and in turn will result in a wide range of physical and mechanical properties, making them suitable for many applications. The density of PUR foam can be controlled by varying the amount of blowing agent, and consequently, properties such as mechanical, morphological, water absorption, thermal behavior and the internal architecture represented in cell size and cell-wall thickness can all be controlled as well (Thirumal *et al.*, 2008). Soft PUR foam is widely used in making furniture, mattresses, and vehicles seats, while rigid PUR foams on the other hand are often used in structural material such as sandwich panels (Chow, 2004; Fam and Sharaf, 2010). In addition, a lot of research work has been conducted to study the thermal behavior of PUR foams. It has been found that PUR foams possess low thermal conductivity and hence are widely used as a thermal insulation material. Albrecht (2000) mentions that the gas exchange between the ambient air and the blowing agent greatly affects the thermal conductivity for closed cell foams. It has been proved that thermal properties of PUR foam can be controlled, and hence, can be widely used in industrial insulation. Li *et al*. (2013) worked on reducing the flammability of polymeric materials by employing the technology of layer-by-layer coating using PUR foam. Using tailoring assembly, flammability is significantly reduced without affecting the mechanical and physical attributes of the PUR foam. Along the same lines, PUR foams are commonly used in the field of acoustics; its high acoustic absorption properties are enough to reduce acoustic reverberation, making it a powerful candidate to be used in the acoustic treatment of auditoriums and other large spaces requiring specific acoustic performance (Ibrahim and Melik, 2003). Moreover, all of the PUR foam densities are light in weight, which makes PUR widely used in aerospace and marine applications (Ekin *et al.*, 2007). Besides, many research studies focus on using PUR material in renewable energy applications. Linul and Marsavina (2013) introduce a construction of wind turbine blades that employs rigid PUR foam as a core material that provides adequate rigidity for the outer thin shell of the blades. Static and dynamic compression tests have been carried out on samples of sandwich beams in order to provide a better understanding of the failure mechanisms conducted to the core materials used in wind turbine blades.

In the field of automotive industry, PUR foams are already used by automotive manufacturers to increase the crashworthiness of automobiles (Lilley and Mani, 1998), by

*Corresponding author. e-mail: amr.ahmed@eng.asu.edu.eg

(1) increasing the bending strength of thin-walled components of the vehicle structure (Sun *et al.*, 2010), and (2) being able to absorb the impact energy due to the material porosity and low filling ratio (Ma *et al.*, 2015). Along the same line, Chen *et al*. (2015) have worked on improving the design of light weight trucks by optimizing crashworthiness by building a finite element model (FE-model) and validating it against cab modal test and frontal impact test. The simulation shows that the cap stiffness is improved, and the energy absorption is homogeneous. In addition, flexible PUR foams are used early on in the design of car seats; their properties are tailored to introduce the appropriate performance that meets the design requirements. Casati *et al*. (1998) have worked on adjusting the cushioning characteristics of flexible PUR foam to obtain a better performance for the foam/seat assembly. Their study is concerned with the optimization of the balance between the foam weights and their other characteristics while simultaneously taking comfort and durability into account. Similarly, Han *et al*. (2014) introduce a study to examine the impact absorption of Aluminum foam when applied to a crash box of a vehicle crashing with low speed. A numerical simulation is carried out and validated to experimental tests. Cho *et al*. (2013) also present similar work but on sandwich composites with Aluminum honeycomb cores.

Several publications have addressed the problem of designing and testing the impact attenuator. Belingardi and Obradovic (2010) have developed numerical simulation of the crash test. A FE-model is developed for an impact attenuator built of two metals: steel and Aluminum with elastic-plastic properties. They conclude that an ideal design of the impact attenuator would involve a material with almost flat force versus time curve. Moreover, they note that large values of deceleration occur at the beginning of the crash, which is due to the initialization of the impact attenuator structure collapse. They perform the analysis in two steps: initial study of the impact attenuator as an independent structure and evaluating the whole performance after adding the assembly of the racing vehicle frame. The results obtained from their analyses fit well with the requirements of SAE 2008 rules. In the same context, Singhal and Subramanium (2013) present a simple, cost effective, intuitive design of an impact attenuator for a Student Formula Racing car and test its effectiveness with drop weight test analysis. They prepare a simple initial design consisting of single step empty shell attenuator, and then they develop the design into two steps shell stuffed with an array of bottles and cans. Although the design is so simple, they have succeeded in providing average deceleration of less than 20g. Another effort in that field was introduced by Obradovic *et al*. (2012). Their study is built upon achieving energy absorption by using material diffuse structure which occurs in composites, rather than using metals at which energy abortion is achieved by plastic deformation. Analytical, experimental, and numerical analyses of the structural crashworthiness have been conducted in order to provide regular and controlled dissipation in kinetic energy.

A major challenge in the field of crashworthiness design is to obtain the optimum crashworthiness while the problem is complex and highly nonlinear. One of the works that focuses on crashworthiness optimization is done by Song *et al*. (2013). The paper presents an optimization process conducted to design a foam-filled tapered thin-walled (TW) structure. A comparative study on 4 types of surrogate models is done to determine the most suitable one for the nonlinear responses. Along the same lines, a broad survey of the field of crashworthiness behavior of the vehicle structure components is introduced by Baroutaji *et al*. (2017). The survey introduced through the paper focuses on the study of the crashworthiness behavior of hollowed and foam-filled TW tubes subjected to axial, bending, and oblique loadings. Different collision scenarios are represented to study the most common loading/deformation modes of TW tubes used in vehicles. All in all, the paper reviews most research work conducted in the field of crashworthiness in the last decade. Finally, an impact attenuator made up of honeycomb sandwich panel is introduced by Coppola *et al*. (2020). The energy absorption capacity at different Aluminum alloys has been studied considering the geometric cavities within the proposed structure. Numerical model has been developed using LS-Dyna, while the Johnson Cook model has been used to model the material behavior. The numerical work has been validated experimentally, and the proposed design has proved to have high maximum energy absorption capacity with optimum geometry. Finally, a study of the crushing response of aluminum tubes of square shapes has been studied when filled with both polyurethane foam and aluminum honeycomb (Hussein *et al*., 2017). The study has proven that the failure mechanism of the tubes depends on the characteristics of the fillers. The fold wavelength, the effect of velocity, and the mean crushing force have all been recorded.

After reviewing the research work discussed above, it is thought that employing the dynamic characteristics of PUR material in designing the impact attenuator of racing vehicles is a good contribution that is worth studying. Besides, none of the literature work has focused on the shape optimization of the internal structure of the attenuator neither using the constant nor the varied wall thickness techniques. Therefore, this paper aims at developing a numerical model which can be used to predict the crashworthiness performance of PUR foam structures when used as impact attenuators in automotive applications and hence can be used to select proper foam density and geometry capable of reducing the impact force. The structure of the research work is illustrated in Figure 1.

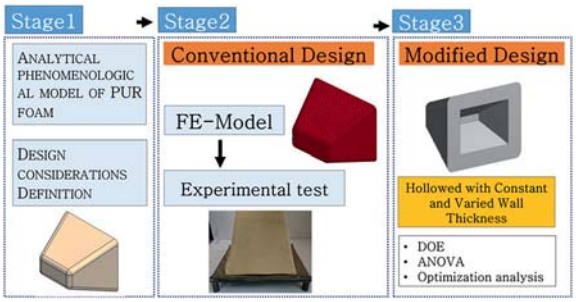

Figure 1. Structure of the research work.

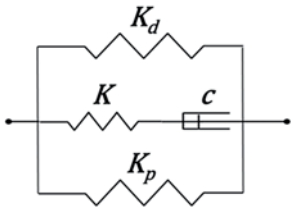

Figure 2. Modeling the elastic, plastic, and densification behaviors of the PUR foam.

2. ANALYTICAL PHENOMENOLOGICAL MODEL OF PUR FOAM

The characteristics of PUR foam can be determined by its density, isotropic elasticity, and strain hardening. The viscoelastic behavior of PUR foam and, consequently, the stress-strain relationship both depend on the foam density (Deshpande and Fleck, 2000; Li *et al*., 2000). The stress strain curve of PUR foam is generally divided into three regions: elastic rise, plastic plateau, and abrupt-densification -rise regions. Based on the theoretical understating of the PUR foam, the behavior of PUR foam through the three regions can be eventually modelled as shown in Figure 2 as described by Vladimir (2010).

In the illustrated model, the stress is distributed among three arms corresponding to the elastic, plateau, and densification states in the PUR foam material. The stiffnesses of the springs and the viscous damping coefficient of the damper correspond to the elastic and plastic behaviors of the foam throughout the three regions, respectively. Based on the study introduced by (Alzoubi *et al*., 2014), the stress and strain expressions for each arm eventually leads to the following relation:

$$\sigma = c\left(-1+e^{\frac{K\in}{c}}\right)e^{\frac{-K\in}{c}} + \in(K_p+\gamma(1-e^{\in})^n) \qquad (1)$$

Where σ and $\in$ denote stress and strain components, (γ) is the factor representing the stress growth rate during densification, ($\in$) is the strain, and (n) is an even exponent that describes how early the densification starts. Many research works have worked on the determination of those constants stated in the last formula via uniaxial compressive tests. It is found that those constants differ according to the foam material and its density. In this paper, the constants which are determined experimentally by Vladimir are used as shown in Table 1, and his experimentally validated formula is employed to obtain the stress-strain curves for various PUR foam densities.

As evident in Figure 3, it can be noticed that the higher the density of the PUR foam, the higher the plateau stress and the lower the densification strain. The PUR densities of interest throughout this study are in the range of 60 to 145 kg/m^3. Densities lower than 60 kg/m^3 are expected to be too soft to withstand impacts. On the other hand, densities higher than 145 kg/m^3 are expected to be too hard to absorb impact energy. The strain at failure for each density are determined from literature (See Vladimir, 2010). The material data obtained in this section is employed throughout the analyses carried out in the rest of the research work.

3. DESIGN CONSIDERATIONS OF THE ATTENUATOR

This section tackles the design considerations associated with impact attenuators in general. Although this study introduces a dimension-independent methodology for designing impact attenuators, the design considerations stated in the SAE® Rules (2020) are considered as an application. According to the guidelines, the average acceleration (a_{av}) of the vehicle should not exceed -20 g, with a peak

Table 1. Material constants used to obtain stress strain relations for various PUR foam densities as obtained by Vladimir (2010).

ρ [kg/m^3]	c [MPa]	K [MPa]	K_p [MPa]	γ [MPa]	n [-]
60	0.71	21.9	0.086	0.369	6
80	1.1	32.4	0.09	0.5	6
100	1.48	45.68	0.09	1.181	6
120	2	53.6	0.094	2	4
145	2.25	60.48	0.1	2.25	4

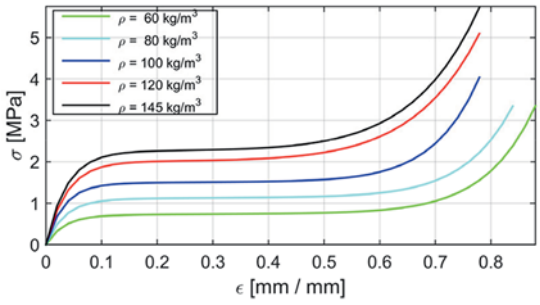

Figure 3. Stress-strain curves obtained from analytical model for different PUR foam densities.

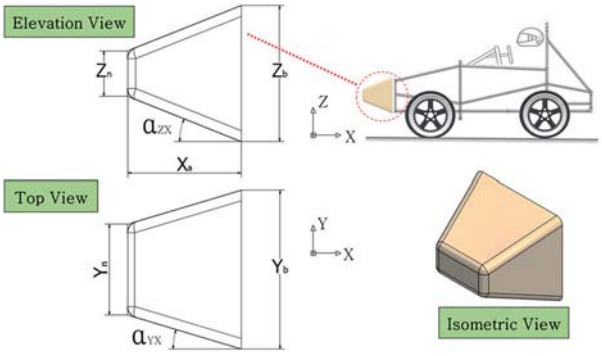

Figure 4. Original design model of the impact attenuator according to the SAE rules.

acceleration (a_{max}) less than or equal to -40 g. The proposed design of the attenuator is presented in Figure 4.

Basically, it is expected that the vehicle's velocity will be decreasing gradually starting from the instant of impact until it reaches zero, when the attenuator will have reached maximum compression, and the acceleration will have reached its maximum value. After reaching rest, velocity starts increasing once more but in the opposite direction, and the acceleration values start decreasing until they reach zero. The instant the acceleration reaches zero is the same instant at which the contact between the attenuator and the barrier ends. Moreover, the studied time interval should be selected to guarantee that the maximum acceleration value will be revealed within it. If the impact attenuator reaching rest exceeds this interval, then this is proof of lack of rigidity, and, consequently, its failure to perform its function, since it will reach a state of damage. In addition, as the average acceleration a_{av} is the main criteria to judge or compare the proposed designs, it should be considered that the average is not calculated along the same time interval for all cases, instead it is calculated from the time at which the impact starts to the time the acceleration returns to zero.

The geometric parameters and the permissible dimensions stated in the guidelines are stated in Table 2. The impact attenuator is about 350 mm wide, 300 mm height, and 250 mm length with inclination angle of 21.8 ° for upper and lower surfaces and 16.7 ° for the sides. Using simple laws of motion, the time to rest is expected to be higher than 0.04 sec, and the total energy absorbed must meet or exceed 7350 J. Accordingly, the attenuator is expected to crash in this case to at least 50 % of its original length.

Being in the front of the racing vehicle, the impact attenuator assembly is usually designed to be tapered (or wedged) for aerodynamics considerations. Unfortunately, this tapered shape negatively affects the stress distribution along the attenuator, which is in turn reflected in the acceleration results. The ratio of least cross-sectional area in the attenuator to the base area is denoted as R_A and can be determined from Equation (2). For better performance of the attenuator, R_A should be adjusted to unity.

$$R_A = \frac{A_n}{A_b} = \frac{(Z_b - 2X_a \tan\alpha_{ZX})(Y_b - 2X_a \tan\alpha_{YX})}{Z_b Y_b} \quad (2)$$

4. FE-SIMULATION OF THE IMPACT TEST

4.1. Basic Setups of the FE-Model

The basic concept of FE-simulations is to provide a virtual model that can replace experimental work while studying

Table 2. Geometric parameters of impact attenuator [Original Model].

Symbol	Description	According to SAE rules
Z_b	Hight of attenuator base.	300 mm
Y_b	Width of attenuator base.	350 mm
X_a	Attenuator Length.	250 mm
Z_n	Hight of attenuator nose.	100 mm
Y_n	Width of attenuator nose.	200 mm
α_{ZX}	Inclination angle in ZX plane.	21.8 °
α_{YX}	Inclination angle in YX plane.	16.7 °
A_b	Area at attenuator base.	105,000 mm^2
A_n	Area at attenuator nose.	20,000 mm^2
R_A	Ratio of least cross-sectional area in the attenuator to A_b.	19 %

each parameter of interest. In this study, the FE-model is developed using LS-Dyna4.3©. As the impact process is an extremely non-linear dynamic process, explicit analysis is selected. One of the essential parameters involved in explicit analyses is the time step, which logically affects the overall running time. The time step is usually selected based on the element of the least quality in the system. Therefore, the FE-model of the attenuator is constructed using solid tetrahedral elements, which are thought to be quite suitable to simulate the behavior of the attenuator throughout the impact period. The rigid barrier – into which the racing vehicle is going to crash – is modeled using quadrilateral elements and is fully constrained. Besides, a 300 kg racing vehicle mass is represented by a mass concentrated at and rigidly connected to the attenuator base which simulates the inertial force of the racing vehicle. The FE-model of the attenuator, rigid barrier, and the vehicle are all presented in Figure 5.

On the other hand, an initial velocity of 7 m/sec is assigned to the mass representing the vehicle and the termination time is set as 0.09 sec to guarantee that the vehicle returns to the opposite direction within the studied time interval. The contact between the attenuator and the rigid barrier is defined using (AUTOMATIC_NODE_TO_SURFACE) which allows the sliding resulting from the lateral strain of the attenuator during impact while prohibiting any penetration between both. Finally, this type of contact guarantees that the contact formulation will remain valid for the interior nodes even after the erosion of the exterior elements.

4.2. Material Modeling

Based on the study carried out by Sambamoorthy and Halder (2001), the material model (MAT_57) available in LS-Dyna 4.3© has proved to be the most accurate one to simulate the behavior of the PUR foam under compression. They have tested four material models and the results obtained when (MAT_57) is used have been found to be quite close to experimental results. This material model requires three basic information: foam density, Young's Modulus, and the nominal stress strain relation, which are all available as discussed in section 2. However, a material failure criterion should be clearly assigned to the material model. As the attenuator is mainly exposed to uniaxial compression in this application, the failure criterion is assumed to be the same as that obtained analytically while a uniform foam block is tested. Accordingly, the material failure criterion is defined as the strain exerted by the foam block at failure through the uniaxial compression test. The (MAT_ADD_ERROSION) available in LS-Dyna4.3© is employed to set the element erosion criterion based on the selected material failure criterion (Barsotti, 2012). By activating this option, the solver eliminates the elements that reach this failure limit out of the model to prevent problematic errors and unrealistic deformed shape (Shah and Topa, 2014).

To evaluate the accuracy of the material model, a FE-simulation of a quasi-static compression test is carried out on a 100 mm cubic PUR foam block using LS-Dyna4.3©. The block is compressed by a strain rate of 0.02 Sec^{-1}. The simulation is repeated for all densities and the stress-strain relation is plotted each time. The different phases through which the block passes are shown in Figure 6. On the other hand, the material model (MAT_RIGID) is found quite suitable for both the rigid barrier and the vehicle. This material model is used for non-yielding parts and allow to define the boundary conditions as a part of the material data. Finally, as the PUR foam block is modeled using hexahedral elements, fully-integrated elements are used to prevent hourglassing (Burbank and Smith, 2012).

The deformation gradients noticeable in Figure 6 may be attributed to the viscous effects in the material model used which creates deformation gradients as a result of the non-zero strain rate.

4.3. FE-Results

Throughout the impact period, the velocity, acceleration, and the impact load are plotted as shown in Figures 7 (a), 7 (b) and 7 (c), respectively. In addition, the damaged attenuator as revealed from the analysis is shown in Figure 7 (d). The analysis is repeated for various PUR densities (ρ): 60, 80, 100, 120 and 145 kg/m^3.

Based on the results shown in Table 3, PUR of density 80 kg/m^3 is characterized by optimal properties in this case. Although the PUR of density 60 kg/m^3 shows better

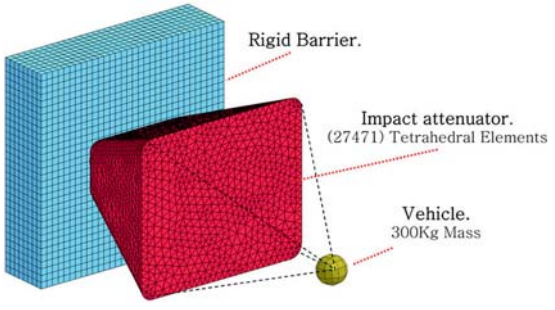

Figure 5. FE-Model of the impact attenuator, rigid barrier, and racing vehicle.

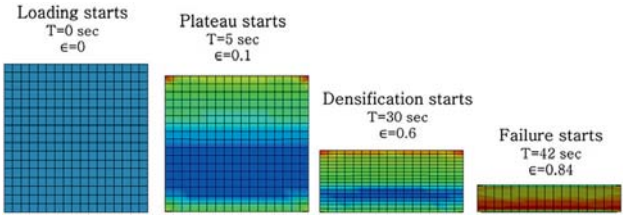

Figure 6. Simulation of a compression test on a 100 mm cubic block of PUR foam of density 80 kg/m^3.

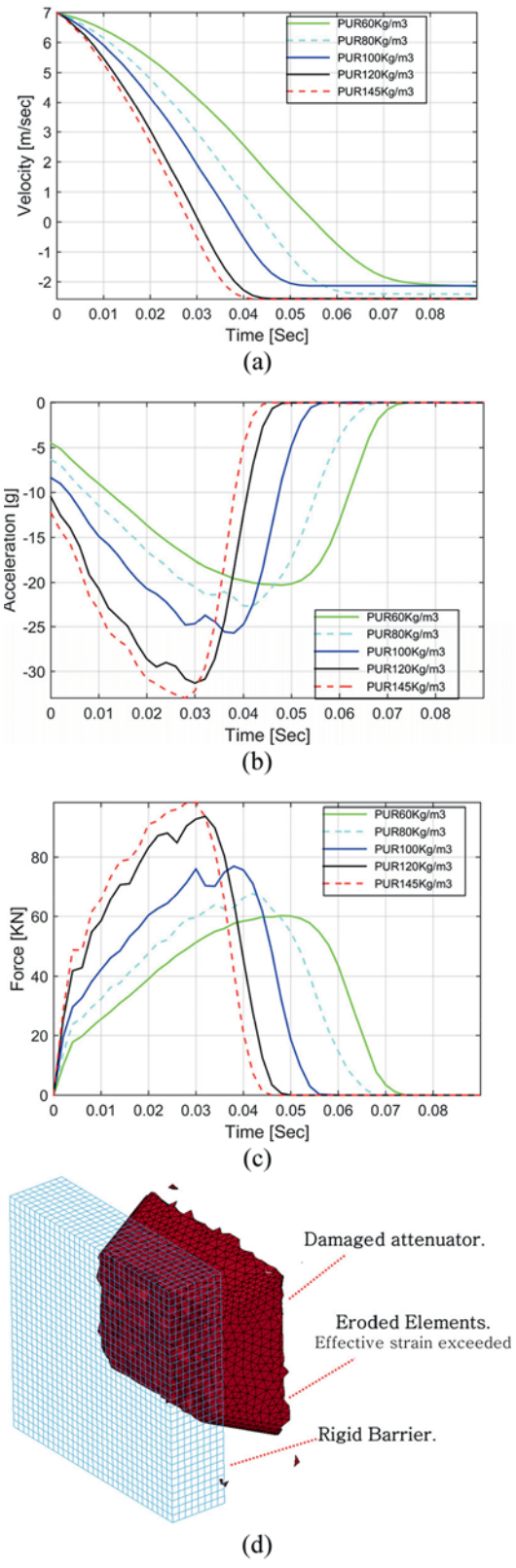

Figure 7. (a) Velocity; (b) Acceleration; (c) Force results for different PUR densities; (d) damaged attenuator as resulted from FE-simulation.

average and maximum acceleration values, the attenuator ends by a damage percentage (λ) of 83 % which is, in terms of safety, critical and not accepted. The damage percentage (λ) represents the percentage of the length of the damaged portion of the attenuator to the original length. Needless to mention that any density below 60 kg/m^3 will lead to a higher λ and consequently, will not be accepted either. For PUR of density 80 kg/m^3, the racing vehicle comes to rest after damage of 72 % of the attenuator and within 0.066 sec. It also yields acceptable average and maximum acceleration values of -14.07 g and -22.65 g respectively, which is within the acceptable limit. Moreover, from the aspect of mass minimization, essential for racing vehicle designs, the 80 kg/m^3 PUR foam has logically the least weight, about 50 % less than that of 145 kg/m^3 PUR foam. Besides, impact load is proved to be minimum in case of 80 kg/m^3 PUR foam, as it shows a maximum impact load (F_{max}) of only 67.71 kN. On the contrary, the PUR foam densities of 120 and 145 kg/m^3 are rejected in this case, as the average acceleration a_{av} exceeds the accepted limit.

Although the results obtained by this PUR foam density meets the design requirements, some design modifications can be achieved to lead the average value to the lowest level possible. Sections 6 and 7 represent the trials performed to achieve the optimum crashworthiness of the attenuator.

5. EXPERIMENT

This section tackles the manufacturing and testing of an impact attenuator to make sure that it conforms with the desired specifications stated previously. For that purpose, it takes place in two stages. Stage 1 is conducting a quasi-static compression test to a cubic block of PUR foam; and stage 2 is conducting a compression test to the impact attenuator manufactured in accordance with the best design model as revealed in the results of the FE-simulation.

5.1. Quasi-Static Compression Test on a PUR Foam Block

The material data that the FE-simulation relies on are derived from the analytical results as stated in section 2. In order to manufacture the impact attenuator, the specifications of the material used in the manufacturing process had to conform to the specifications used as input for the FE-solver. For that purpose, an 80 kg/m^3 PUR foam cubic block of 100 mm edge length is prepared, and a quasi-static compression test is performed. The foam block is subjected to compression with a steady rate of 0.02 sec^{-1} to eliminate the inertial effects. A FE-simulation for the quasi-static compression test is carried out by simulating the low-rate compression acting on a virtual model of the foam block with the same dimensions. The stress-strain curve generated form the FE-simulation of the test is compared to that obtained from the experiment as shown in Figure 8 and they both show a satisfying similarity.

Table 3. FE-results for the impact attenuator at various PUR foam densities.

ρ [kg/m^3]	a_{av} [g]	a_{max} [g]	Time to zero acc. [Sec]	Damage [%]	Mass [kg]
60	-13.12	-20.29	0.072	83	0.854
80	-14.07	-22.65	0.066	72	1.138
100	-16.79	-25.7	0.054	62	1.423
120	-20.63	-31.3	0.046	49	1.707
145	-22.48	-32.94	0.042	46	2.063

5.2. Manufacturing and Testing the Recommended Design of Impact Attenuator

An impact attenuator has been manufactured in accordance with the design model that yielded the best results in the previous analysis. An attenuator has been manufactured out of 80 kg/m^3 PUR foam. Although the drop weight impact test is the most accurate in this case, the impact energy (7350 J) requires a huge drop weight impact test machine on which a 300 Kg should be dropped from about 2.5 m height, and this is not available. Instead, as allowed by the SAE rules, a compression test is conducted to test the impact attenuator as shown in Figure 9 (a). The results of the experiment have been compared to the FE-simulation results of the dynamic test, as shown in Figure 9 (b). The experimental results have shown a dissimilarity but within accepted limit, which are believed to be due the different nature of compression test and dynamic impact test.

In the FE-simulation, the foam is modeled using the material model (MAT_57), therefore the actual behavior of the PUR foam under dynamic compression load is captured. At higher strain rates, the viscoelastic characteristics of the PUR foam lead the attenuator to show higher stress values, if compared to the low rate of the static compression load case (Sadighi and Salami, 2012). This explains the dissimilarity in the experimental and numerical load-displacement results. However, this deviation is limited to the intermediate region only. The identicality that appeared in both experimental and the numerical results at low and high displacement values proves that the foam, anyway, follows the same Young' modulus and ultimate strength. The experimental results show that the load reaches maximum value of 66.86 kN at displacement 180.52 mm, while the FE-results show a maximum load of 67.71 kN at displacement 181.48 mm. This small deviation proves that the FE-results are verified, and the developed FE-model is reliable. Finally, for more confirmation of the FE-model validity, a FE- simulation is carried out yet, based on static compression. As shown in Figure 9 (b), in this case, the results show great similarity to the experimental results.

6. HOLLOWED ATTENUATOR MODEL WITH A CONSTANT THICKNESS

By observing the acceleration results generated while testing

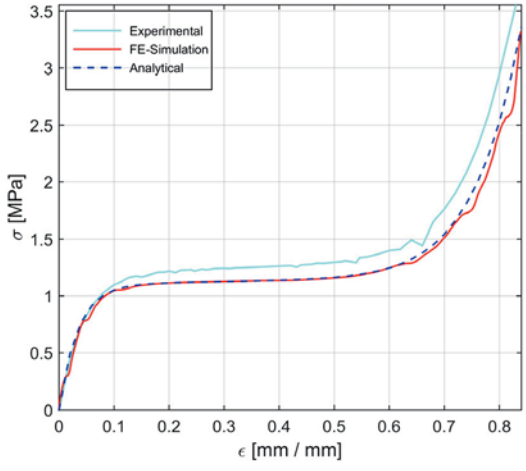

Figure 8. Stress strain relation obtained experimentally and by FE-simulation of a quasi-static compression test for a cubic block of 80 kg/m^3 PUR foam.

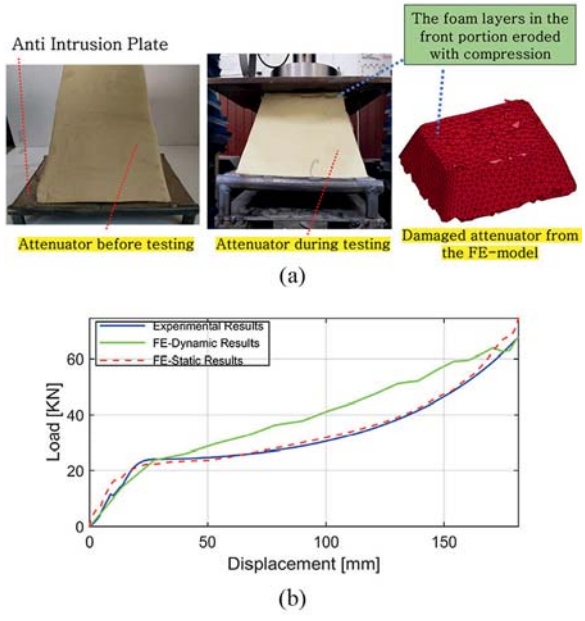

Figure 9. (a) Tested model of the impact attenuator; (b) Experimental and FE-simulation results: Load/Displacement of the impact attenuator.

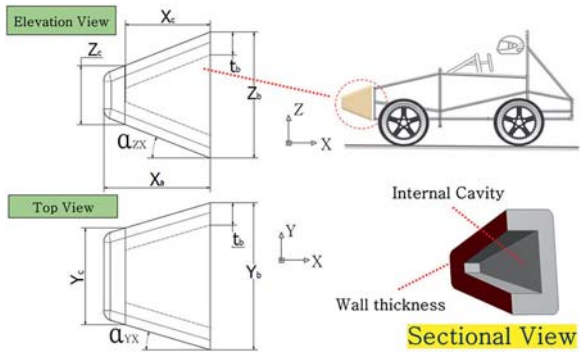

Figure 10. Modified design model of attenuator: cavity with constant thickness.

Table 4. Geometric parameters of impact attenuator with modified topology [Hollowed with constant thickness].

Symbol	Description
X_c	Internal cavity depth.
t_b	Thickness of the wall at attenuator base.
Z_c	Height of attenuator cross section at cavity end.
Y_c	Width of attenuator cross section at cavity end.
A_c	Area of attenuator cross-section at cavity end.

different PUR foam densities, it can be noticed that the acceleration trend line reaches the maximum peak value when the velocity reaches zero. A curve in which the acceleration is almost constant along the impact time interval would have been more favorable and can better satisfy the design requirements; this can be indicated by calculating the standard deviation (σ_d) of the acceleration values beside the average value. Although, the stress-strain curve of the foam itself shows a plateau of stress, the original solid design of the impact attenuator does not show a similar response because its cross-sectional area is linearly varying. The varying cross-section area results in a nonhomogeneous stress distribution along the attenuator, as well as localized compressive stresses on the front portion. Therefore, as an attempt to achieve a better performance of the impact attenuator, a modification has been conducted to the topology of the attenuator in which a tapered cavity has been introduced inside as a trial to maximize the ratio R_A. The proposed modified model of the attenuator is presented in Figure 10.

The dimensions of the cavity are defined in terms of the thickness of the wall at the attenuator base t_b, and the internal depth X_c, so the inside surfaces of the cavity will remain parallel to the outside surfaces of the impact attenuator. The geometric parameters related to the proposed design is defined in Table 4.

The value of R_A in this case can be calculated from Equation (3), and it is obviously greater than that in the case of solid model, whatever the cavity size. Besides, the depth of the cavity X_c is limited according to Equation (4), which indicates the depth value at which the area of the cavity will become zero.

$$R_A = \frac{A_c}{A_b} = 1 - \frac{2X_c(\tan\alpha_{ZX} + \tan\alpha_{YX})}{Z_b + Y_b - 2t_b} \quad (3)$$

$$L_c < Min\left(\frac{Z_b - 2t_b}{2\tan\alpha_{ZX}}; \frac{Y_b - 2t_b}{2\tan\alpha_{YX}}\right) \quad (4)$$

6.1. DOE for the Hollowed Attenuator with Constant Thickness

Basically, if the cavity is not large enough, it does not lead to any notable improvement; if it is too large; it softens the impact attenuator and leads to worse results. Accordingly, size optimization analysis is conducted in order to select the optimum topology for the cavity that would yield the best results. A DOE based on full factorial design is selected for this study using Minitab19©. Two controllable input variables are defined, which are the thickness at the base of the attenuator t_b, and the foam density ρ. Five design levels are defined for the t_b ranging from 60 mm to 100 mm, with a step of 10 mm. As for the other input variable, the density, four levels are defined as 80, 100, 120, and 145 kg/m^3.

It is worth mentioning that DOE usually is recently a starting point of a subsequent optimization. Optimization techniques such as [Desirability, genetic algorithm, particle swarm, etc..] usually are used in combination of regression models such as [response surface or Taguchi]. However, in this research work, the factorial design has been chosen because it produces discrete values for the design variable (the thickness). Obtaining continuous values from the optimization requires more costly techniques for manufacturing the impact attenuator and measuring its dimensions. It is not expected that this additional cost would lead to any significant improvement in the performance.

On the other hand, the response variables of interest are the average acceleration a_{av}, the maximum acceleration a_{max}, the standard deviation σ_d, the maximum impact load F_{max}, and the damage percentage (λ). The DOE has resulted in 20 tests each has a specific combination of the controllable input variables. The FE-simulation is carried out for each test and the generated results are presented in Table 5.

Table 6 shows the analysis of variance (ANOVA) table including the degree of freedom (DF), the adjusted sum of squares (Adj SS), and the adjusted mean squares (Adj MS), for both a_{av} and a_{max}. Generally, in most of the studied samples, results show improvement in the attenuator performance for all PUR foam densities if compared to the original solid model. However, some design models show results that do not conform with the design requirements. For example, the design models of small t_b are rejected when 80 kg/m^3 PUR foam is used, as the lack of rigidity that has resulted from the large internal cavity leads to a total damage without any considerable energy absorption.

Table 5. Full factorial design analysis for the modified attenuator [Hollowed with constant thickness].

Test No.	t_b [mm]	ρ [kg/m^3]	a_{av} [g]	a_{max} [g]	σ_d	F_{max} [kN]	λ [%]
1	100	100	-10.04	-23.97	7.88	71.08	0.66
2	80	100	-10.15	-20.18	5.68	60.20	0.70
3	70	120	-10.99	-19.41	5.77	57.25	0.64
4	90	80	-10.20	-18.38	6.31	54.90	0.80
5	90	120	-18.08	-29.09	9.74	86.08	0.52
6	70	100	-11.07	-32.21	9.36	95.84	0.82
7	80	145	-19.27	-28.17	8.73	83.30	0.48
8	80	120	-17.06	-26.01	8.19	76.68	0.53
9	100	80	-10.17	-18.28	6.28	53.93	0.82
10	60	145	-9.70	-41.54	9.83	131.6	0.78
11	80	80	-10.57	-23.16	7.35	68.28	0.84
12	60	80	-15.99	-45.31	15.10	134.9	0.93
13	60	100	-14.64	-48.82	15.48	146.6	0.88
14	90	100	-11.78	-22.16	7.19	66.31	0.67
15	100	145	-21.31	-33.43	10.80	99.61	0.45
16	60	120	-10.73	-40.83	10.61	121.1	0.81
17	100	120	-20.74	-30.76	9.30	91.17	0.48
18	90	145	-17.94	-31.07	11.14	91.78	0.48
19	70	145	-15.99	-23.65	7.17	70.68	0.55
20	70	80	-13.74	-33.82	10.02	99.62	0.90

Table 6. ANOVA table for the modified impact attenuator [Hollowed with constant thickness].

Terms		DF	Adj SS		Adj MS	
			a_{av}	a_{max}	a_{av}	a_{max}
Linear	t_b	4	21.59	1088.52	5.39	272.13
	ρ	3	99.67	36.47	33.22	12.16
2-Way interactions	t_b*ρ	12	178.36	428.31	14.86	35.69
Total		19	299.6	1553.29	-	-

On the contrary, the design models of large t_b show the least improvement when this model is used with 145 kg/m^3 density, though it is rather because of their high rigidity.

6.2. Optimization Analysis

To obtain the optimum design model, the objective function should be first defined. According to the design considerations, the objective function is to minimize a_{av} and σ_d, while a_{max} and λ values are set as constraints so that they would not exceed -40 g and 80 %, respectively. Based on the optimization analysis, the optimum design model is found to be the one that has t_b of 80 mm and density of 100 kg/m^3. The corresponding a_{av}, a_{max}, and σ_d are -10.15 g, -20.18 g, and 5.68, respectively. This indicates lower values for a_{av}, a_{max}, and σ_d by 27.8 %, 10.9 %, and 15.22 %, respectively, if compared to the original solid model.

Besides, the F_{max} for this model is found as 60.2 kN, which is 11.1 % less than it in the original solid model. The mass is also reduced by 13.4 % if compared to the solid attenuator of the same PUR density. The best five acceleration results of the constant thickness design model are shown in Figure 11.

7. HOLLOWED ATTENUATOR MODEL WITH A VARIED THICKNESS

In this section, another attempt to improve the attenuator performance is discussed. Similar to the previous section, an internal cavity is added to the attenuator, yet with a varied wall thickness. The main purpose of varying the thickness is to maintain the cross-sectional area constant along the greatest possible part of the attenuator length, which results in a R_A value of unity. The proposed design of the hollowed attenuator with varied thickness is presented in Figure 12, while the geometric parameters involved in this design model are presented in Table 7.

The wall thickness of the attenuator at an arbitrary length X_i is defined as t_i. At the attenuator base, X_i is equal to zero, and hence, the t_i is equal to t_b. As the cross-sectional area is intended to be constant as stated in Equation (5), the

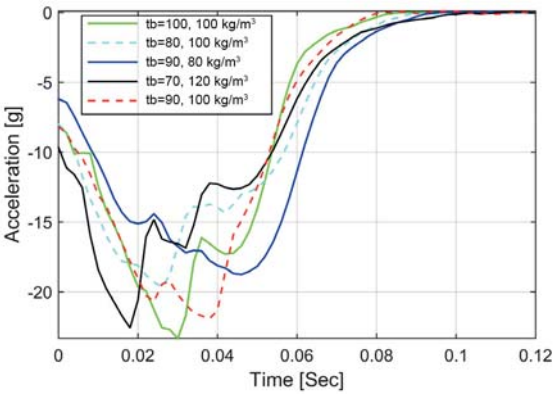

Figure 11. Acceleration results for five different design models of the hollowed attenuator with constant thickness at different PUR foam densities.

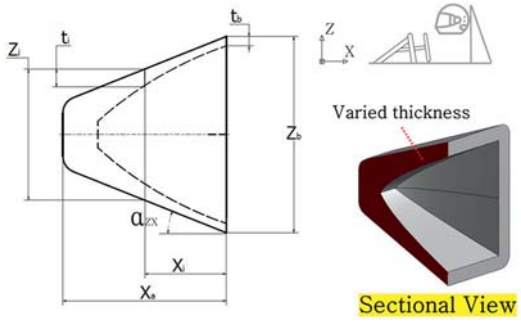

Figure 12. Modified design model of attenuator: hollowed with varied thickness.

Table 7. Geometric parameters of impact attenuator with constant cross-sectional area along length.

Symbol	Description
X_i	Arbitrary depth of attenuator cavity.
X_{imax}	Maximum allowable depth of attenuator cavity.
Z_i	Height of attenuator cross section at depth L_i.
Y_i	Width of attenuator cross section at depth L_i.
t_i	Thickness of the attenuator wall at depth L_i.

thickness t_i is found to follow a polynomial function in terms of X_i, as proved in Equations (6) and (7). However, Equations (8) ~ (10) show that for every specific value of t_b, there is a certain limit of cavity depth X_{imax} that cannot be exceeded. The higher the value of t_b, the lower the value of X_{imax}, and hence, the attenuator approaches the original solid design.

$$A_i = A_b = 2t_i(Z_i + Y_i) - 4t_i^2 \tag{5}$$

$$t_i = \frac{\gamma \mp \sqrt{\gamma^2 - 16A_b}}{8} \tag{6}$$

$$\gamma = 2[Z_b + Y_b - 2X_i(\tan\alpha_{ZX} + \tan\alpha_{ZY})] \tag{7}$$

$$X_{imax} = \frac{\beta \mp \sqrt{\beta^2 - 4\varepsilon}}{2} \tag{8}$$

$$\beta = \frac{(Z_b \tan\alpha_{YX} + Y_b \tan\alpha_{ZX})}{2\tan\alpha_{YX}\tan\alpha_{ZX}} \tag{9}$$

$$\varepsilon = \frac{Z_b Y_b - A_b}{4\tan\alpha_{YX}\tan\alpha_{ZX}} \tag{10}$$

7.1. DOE for the Hollowed Attenuator with Varied Thickness

A DOE based on full factorial design is selected with two controllable input variables, which are the t_b, and ρ. Four design levels are defined for the t_b ranging from 30 mm to 60 mm, with a step of 10 mm. The lower level is set to 30 mm as the attenuator is thought to act very softly if the value of t_b is less than this limit. On the other side, when t_b equals 60 mm, X_{imax} is equal to 100.55 mm, which is about 40 % of the total length. Consequently, if t_b exceeds 60 mm, the X_{imax} will be even lower, and the attenuator tends to act similarly to the solid original model. In addition, four levels are defined for the density as 80, 100, 120, and 145 kg/m^3. The DOE has resulted in 16 tests, each has a specific combination of the two controllable input variables. The FE-simulation is carried out for each test and the generated results are presented in Table 8.

In general, the varied thickness design model is proved to have a better performance if compared to the one of constant thickness. By comparing the results of the whole population of both design models, it can be observed that the average of both a_{max} and σ_d are found to be decreased by 15.18 % and 17.9 % in case of varied thickness design model, respectively. This indicates that the varied thickness design model is a more robust design. The ANOVA table for the varied thickness design model is shown in Table 9.

7.2. Optimization Analysis

The optimization process is carried out similar to the previous section. The optimum design model is found to be the one that has t_b of 30 mm and density of 145 kg/m^3. The corresponding a_{av} and a_{max} are -9.77 g and -19.82 g, respectively, while the σ_d is 4.49. While this indicates insignificant improvement for a_{av} and a_{max} if compared to the constant thickness model (3.7 % and 1.78 % respectively), a significant improvement shows in σ_d by 20.95 %. The best five acceleration results of the varied thickness design model are shown in Figure 13.

8. DESIGN MODEL OF OPTIMUM CRASHWORTHINESS

The optimum design candidates elected from each of the

Table 8. Full factorial design analysis for the modified attenuator [Hollowed with varied thickness].

Test No.	t_b [mm]	ρ [kg/m^3]	a_{av} [g]	a_{max} [g]	σ_d	F_{max} [kN]	λ [%]
1	40	120	-10.73	-18.38	5.73	55.2	0.65
2	30	100	-12.85	-38.49	10.07	118.5	0.91
3	50	80	-10.46	-23.59	6.96	69.8	0.86
4	40	145	-11.56	-21.32	7.13	63.7	0.55
5	60	145	-20.78	-31.61	10.43	94.1	0.44
6	60	80	-10.58	-17.99	5.89	53.3	0.77
7	50	100	-10.07	-21.55	4.80	48.6	0.74
8	40	80	-10.42	-27.77	8.57	83.2	0.90
9	30	120	-9.93	-20.11	5.43	59.8	0.84
10	30	145	-9.77	-19.82	4.49	42.91	0.78
11	50	120	-16.82	-23.58	8.02	70.50	0.53
12	50	145	-19.29	-26.75	8.35	79.53	0.47
13	60	120	-19.23	-29.21	9.83	86.94	0.48
14	60	100	-14.51	-22.43	8.19	66.54	0.60
15	30	80	-12.51	-36.29	10.40	111.16	0.98
16	40	100	-11.07	-21.68	5.25	56.83	0.78

Table 9. ANOVA table for the modified impact attenuator [Hollowed with varied thickness].

Terms		DF	Adj SS		Adj MS	
			a_{av}	a_{max}	a_{av}	a_{max}
Linear	t_b	3	76.82	89.06	25.61	29.69
	ρ	3	46.45	31.29	15.48	10.43
2-Way interactions	t_b* ρ	9	90.8	452.12	10.09	50.24
Total		15	214.07	572.46	-	-

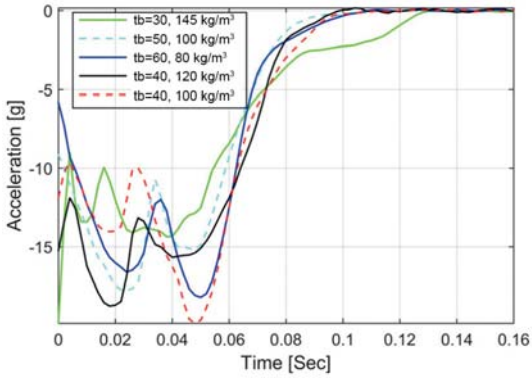

Figure 13. Acceleration results for five different varied thickness design models of the impact attenuator for different PUR foam densities.

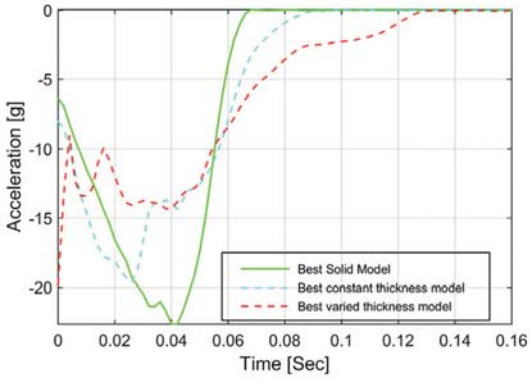

Figure 14. Acceleration results of the best attenuator design models: Solid (ρ=80 kg/m^3), hollowed with constant thickness model (t_b=80 mm, ρ=100 kg/m^3), and hollowed with varied thickness model (t_b=30 mm, ρ=145 kg/m^3).

three studied design models are compared to each other; the solid design model, the constant, and varied thickness design models. Undoubtedly, the optimum acceleration curve is the one that has a peak in the beginning of the event, which indicates that the acceleration starts to decrease by the instant the attenuator touches the barrier. Thereby, as shown in Figure 14, the acceleration pattern for the optimum design candidate of the varied thickness model with 30 mm base thickness and constructed of 145 kg/m^3 PUR is the closest one to the desired pattern. Moreover, If compared to the original solid model, the values of a_{av}, a_{max}, σ_d are less

by 30.56 %, 12.49 %, and 32.98 %, respectively. However, although the varied thickness design model shows better performance in general, the constant thickness design model may be better in terms of manufacturing cost and time.

9. CONCLUSION

In this paper, the crashworthiness optimum design of a PUR foam energy absorber used in racing vehicles is presented. Initially, an analytical model is used to obtain the mechanical properties of the PUR foam of different densities. Thereafter, a conventional design of an impact attenuator fully constructed of PUR foam is simulated using several densities within range 60 ~ 145 kg/m^3. The FE-results show that the attenuator manufactured out of 80 kg/m^3 density can meet the required performance efficiently. The attenuator has been manufactured and tested for validation. An attempt to enhance the performance has been made to modify the topology of the attenuator by introducing an internal cavity with a constant wall thickness. Thus, an optimization analysis is performed to find out the best modification to the topology that makes the attenuator conform the most to the standards. The best candidate for this has been found to be the one that has t_b of 80 mm and density of 100 kg/m^3. Moreover, another attempt has been carried out by adding an internal cavity, yet with a varied wall thickness as a trial to attain a stable acceleration curve. The best candidate for this design model has been found to be the one that has t_b of 30 mm and density of 145 kg/m^3. Finally, the best candidates of each of the three design models are presented against each other, and the varied thickness model has been proved to be the one of best performance.

The proposed methodologies can be extended to other applications such as the design of impact absorbing helmets and aircraft data recorders. Moreover, applying other optimization techniques such as genetic algorithms in conjunction with response surface model can be more efficient in future work. Another recommended future research work is to involve the manufacturing considerations including the cost in the crashworthiness optimization process, as a trial to introduce a comprehensive multi-disciplinary study.

REFERENCES

Albrecht, W. (2000). Cell-gas composition-An important factor in the evaluation of long-term thermal conductivity in closed-cell foamed plastics. *Cellular Polymers* **19**, **5**, 319–332.

Alzoubi, M. F., Al-Hallaj, S. and Abu-Ayyad, M. (2014). Modeling of compression curves of flexible polyurethane foam with variable density, chemical formulations and strain rates. *J. Solid Mechanics* **6**, **1**, 82–97.

Baroutaji, A., Sajjia, M. and Olabi, A. (2017). On the crashworthiness performance of thin-walled energy absorbers: Recent advances and future developments. *Thin-Walled Structures*, **118**, 137–163.

Barsotti, M. (2012). Comparison of FEM and SPH for modeling a crushable foam aircraft arrestor bed. *11th Int. LS-DYNA® Users Conf.*, Detroit, MI, USA.

Belingardi, G. and Obradovic, J. (2010). Design of the impact attenuator for a formula student racing car: numerical simulation of the impact crash test. *J. Serbian Society for Computational Mechanics* **4**, **1**, 52–65.

Burbank, S. D. and Smith, L. V. (2012). *Dynamic characterization of rigid polyurethane foam used in FEA softball simulations*. M. S. Thesis. Washington State University. Pullman, WA, USA.

Casati, F. M., Herrington, R. M., Broos, R. and Miyazaki, Y. (1998). Tailoring the performance of molded flexible polyurethane foams for car seats. *J. Cellular Plastics* **34**, **5**, 430–466.

Chen, D. Y., Wang, L. M., Wang, C. Z., Yuan, L. K., Zhang, T. Y. and Zhang, Z. Z. (2015). Finite element based improvement of a light truck design to optimize crashworthiness. *Int. J. Automotive Technology* **16**, **1**, 39–49.

Cho, J. U., Choi, H. K., Lee, S., Cho, C. and Han, M. S. (2013). Experimental study of the impact characteristics of sandwich composites with aluminum honeycomb cores. *Int. J. Automotive Technology* **14**, **3**, 415–421.

Chow, W. K. (2004). Fire hazard assessment on polyurethane sandwich panels for temporary accommodation units. *Polymer Testing* **23**, **8**, 973–977.

Coppola, L., De Marco, B., Niola, V., Sakhnevych, A. and Timpone, F. (2020). Impact attenuator optimum design for a FSAE racing car by numerical and experimental crash analysis. *Int. J. Automotive Technology* **21**, **6**, 1339–1348.

Deshpande, V. S. and Fleck, N. A. (2000). Isotropic constitutive models for metallic foams. *J. Mechanics and Physics of Solids* **48**, **6-7**, 1253–1283.

Doyle, E. N. (1971). *The development and use of polyurethane products*. McGraw-Hill. New York, NY, USA.

Ekin, A., Webster, D. C., Daniels, J. W., Stafslien, S. J., Cassé, F., Callow, J. A. and Callow, M. E. (2007). Synthesis, formulation, and characterization of siloxane–polyurethane coatings for underwater marine applications using combinatorial high-throughput experimentation. *J. Coatings Technology and Research* **4**, **4**, 435–451.

Fam, A. and Sharaf, T. (2010). Flexural performance of sandwich panels comprising polyurethane core and GFRP skins and ribs of various configurations. *Composite Structures* **92**, **12**, 2927–2935.

Ferrigno, T. H. (1967). *Rigid Plastics Foams*. (2nd edn). Reinhold Publishing Corporation. New York, NY, USA.

Formula SAE® Rules (2020). https://www.fsaeonline.com/cdsweb/app/NewsItem.aspx?NewsItemID=2c1ab552-40c3-4b97-a258-582dca0ea505

Han, M. S., Min, B. S. and Cho, J. U. (2014). Fracture properties of aluminum foam crash box. *Int. J. Automotive*

Technology **15**, **6**, 945-951.

Hussein, R. D., Ruan, D., Lu, G., Guillow, S. and Yoon, J. W. (2017). Crushing response of square aluminium tubes filled with polyurethane foam and aluminium honeycomb. *Thin-Walled Structures*, **110**, 140–154.

Ibrahim, M. A. and Melik, R. W. (2003). Optimized sound absorption of a rigid polyurethane foam. *Archives of Acoustics* **28**, **4**, 305–312.

Li, Q. M., Mines, R. A. W. and Birch, R. S. (2000). The crush behaviour of Rohacell-51WF structural foam. *Int. J. Solids and Structures* **37**, **43**, 6321–6341.

Li, Y. C., Kim, Y. S., Shields, J. and Davis, R. (2013). Controlling polyurethane foam flammability and mechanical behaviour by tailoring the composition of clay-based multilayer nanocoatings. *J. Materials Chemistry A* **1**, **41**, 12987–12997.

Lilley, K. and Mani, A. (1998). Roof-crush strength improvement using rigid polyurethane foam. *SAE Trans.*, 374–384.

Linul, E. and Marsavina, L. (2013). Mechanical characterization of rigid pur foams used for wind turbine blades construction. *Recent Advances in Composite Materials for Wind Turbines Blades.* World Academic Publishing (WAP). Hong Kong.

Ma, C. C., Lan, F. C., Chen, J. Q., Liu, J. and Zeng, F. B. (2015). Automobile crashworthiness improvement by energy-absorbing characterisation of aluminium foam porosity. *Materials Research Innovations* **19**, **sup1**, S1-109–S101-112.

Obradovic, J., Boria, S. and Belingardi, G. (2012). Lightweight design and crash analysis of composite frontal impact energy absorbing structures. *Composite Structures* **94**, **2**, 423–430.

Oertel, G. and Abele, L. (1994). *Polyurethane Handbook.* 2nd edn. Hanser Gardner Publications. Munich, Germany.

Sadighi, M. and Salami, S. (2012). An investigation on low-velocity impact response of elastomeric & crushable foams. *Open Engineering* **2**, **4**, 627–637.

Sambamoorthy, B. and Halder, T. (2001). Characterization and component level correlation of energy absorbing (EA) polyurethane foams (PU) using LS-DYNA material models. *3rd LS-DYNA European Conf*. Paris, France.

Shah, Q. H. and Topa, A. (2014). Modeling large deformation and failure of expanded polystyrene crushable foam using LS-DYNA. *Modelling and Simulation in Engineering*, **2014**, 292647.

Singhal, A. and Subramanium, V. S. (2013). Cost effective and innovative impact attenuator for formula SAE car with drop test analysis. *Int. J. Scientific and Research Publications* **3**, **3**, 1–4.

Song, X., Sun, G., Li, G., Gao, W. and Li, Q. (2013). Crashworthiness optimization of foam-filled tapered thin-walled structure using multiple surrogate models. *Structural and Multidisciplinary Optimization* **47**, **2**, 221–231.

Sun, G., Li, G., Hou, S., Zhou, S., Li, W. and Li, Q. (2010). Crashworthiness design for functionally graded foam-filled thin-walled structures. *Materials Science and Engineering: A* **527**, **7-8**, 1911–1919.

Szycher, M. (2012). *Szycher's Handbook of Polyurethanes*. (2nd edn). CRC press. Boca Raton, FL, USA.

Thirumal, M., Khastgir, D., Singha, N. K., Manjunath, B. S. and Naik, Y. P. (2008). Effect of foam density on the properties of water blown rigid polyurethane foam. *J. Applied Polymer Science* **108**, **3**, 1810–1817.

Vladimir, G. (2010). Testing and application of new phenomenological material model for foam materials. http://www.posterus.sk.